AAS 13-095

OSIRIS-REx Touch-And-Go (TAG) Mission Design and Analysis

Kevin Berry*, Brian Sutter†, Alex May†, Ken Williams‡, Brent W. Barbee*, Mark Beckman*, and Bobby Williams‡

*NASA/GSFC, †Lockheed Martin, ‡KinetX, Inc.

36th ANNUAL AAS GUIDANCE AND CONTROL CONFERENCE

February 1 - February 6, 2013
Breckenridge, Colorado

Sponsored by
Rocky Mountain Section

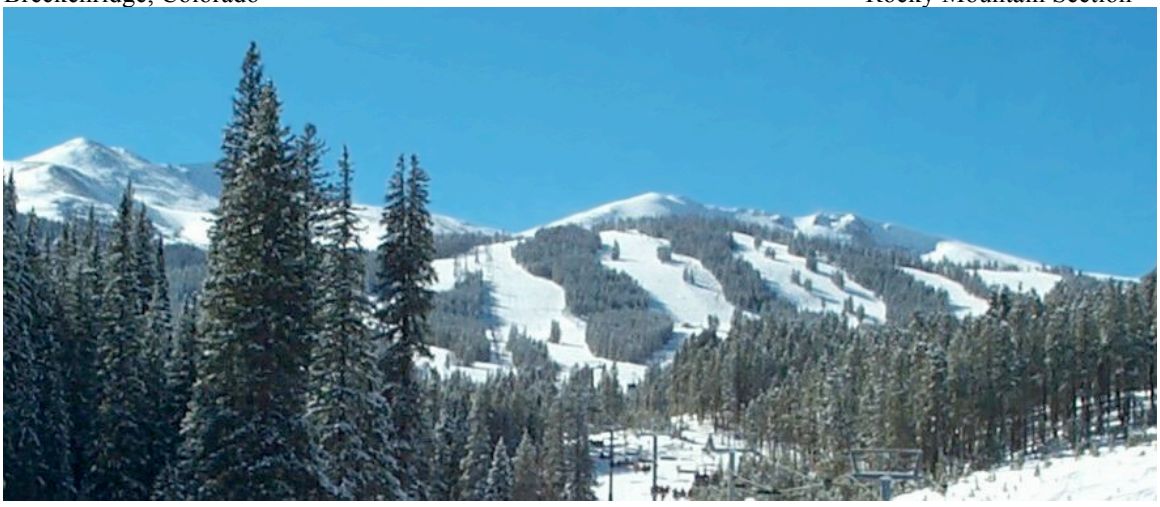

AAS Publications Office, P.O. Box 28130 - San Diego, California 92198

AAS 13-095

OSIRIS-REX TOUCH-AND-GO (TAG) MISSION DESIGN AND ANALYSIS

Kevin Berry[*], Brian Sutter[†], Alex May[‡], Ken Williams[§], Brent W. Barbee[¶], Mark Beckman[‖], and Bobby Williams[**]

The Origins Spectral Interpretation Resource Identification Security Regolith Explorer (OSIRIS-REx) mission is a NASA New Frontiers mission launching in 2016 to rendezvous with the near-Earth asteroid (101955) 1999 RQ_{36} in late 2018. After several months in formation with and orbit about the asteroid, OSIRIS-REx will fly a Touch-And-Go (TAG) trajectory to the asteroid's surface to obtain a regolith sample. This paper describes the mission design of the TAG sequence and the propulsive maneuvers required to achieve the trajectory. This paper also shows preliminary results of orbit covariance analysis and Monte-Carlo analysis that demonstrate the ability to arrive at a targeted location on the surface of RQ_{36} within a 25 meter radius with 98.3% confidence.

INTRODUCTION

Origins Spectral Interpretation Resource Identification Security Regolith Explorer (OSIRIS-REx) is the third mission selected as part of NASA's New Frontiers Program. OSIRIS-REx will travel to a near-Earth carbonaceous asteroid, (101955) 1999 RQ_{36}, study it in detail, and return to Earth with a regolith sample. This sample will provide insight into the initial states of planet formation and the origin of life. The data collected at the asteroid will also improve our understanding of asteroids that can impact Earth.[1]

Upon arriving at the asteroid, the spacecraft will spend 4 months in various orbits collecting surface images, LIDAR data, and radiometric tracking data. The various data sets will be used to develop a detailed topographic surface map, a spin state model, and a gravity model, all of which will be used to select 4 candidate sampling sites on the asteroid's surface.

[*] Aerospace Engineer, NASA/GSFC, Code 595, 8800 Greenbelt Road, Greenbelt, MD 20771, USA.
[†] Senior Staff Engineer, Lockheed Martin Space Systems Company, Systems Engineering, Mission Design, PO Box 179, Denver CO, 80201, MS S8110
[‡] Systems Engineer, Lockheed Martin Space Systems Company, Systems Engineering, 12257 South Wadsworth Blvd, Littleton, CO 80125, USA.
[§] Navigation Team Chief for OSIRIS-REx Mission, KinetX, Inc., Space Navigation and Flight Dynamics (SNAFD) Practice, 21 W. Easy St., Suite 108, Simi Valley, CA 93065
[¶] Aerospace Engineer, NASA/GSFC, Code 595, 8800 Greenbelt Road, Greenbelt, MD 20771, USA.
[‖] Flight Dynamics Systems Manager for OSIRIS-REx Mission, NASA GSFC, Code 595, 8800 Greenbelt Road, Greenbelt, MD 20771, USA.
[**] Director of SNAFD, KinetX, Inc., Space Navigation and Flight Dynamics (SNAFD) Practice, 21 W. Easy St., Suite 108, Simi Valley, CA 93065

The spacecraft will then spend 2.5 months conducting reconnaissance of the candidate sample sites at lower altitudes. The various maps and models will be refined for the regions surrounding the candidate sites and the single best site will be selected for sampling.

The sample will be obtained during the TAG (Touch And Go) sequence, after a series of methodical and incremental TAG rehearsals are completed during a 1.5 month period leading up to the actual TAG.

THE TAG SEQUENCE

The spacecraft begins the TAG sequence in the "Safe Home Orbit," which is a circular solar terminator plane orbit with a radius of 1 km. The orbit departure latitude is chosen to be the negative of the TAG site latitude. When the spacecraft crosses the orbit departure latitude on the morning side of the asteroid, the de-orbit burn will be performed with the goal of arriving at the 125 m altitude Checkpoint position 4 hours later. The trajectory sequence following the de-orbit maneuver is depicted in Figure 1.

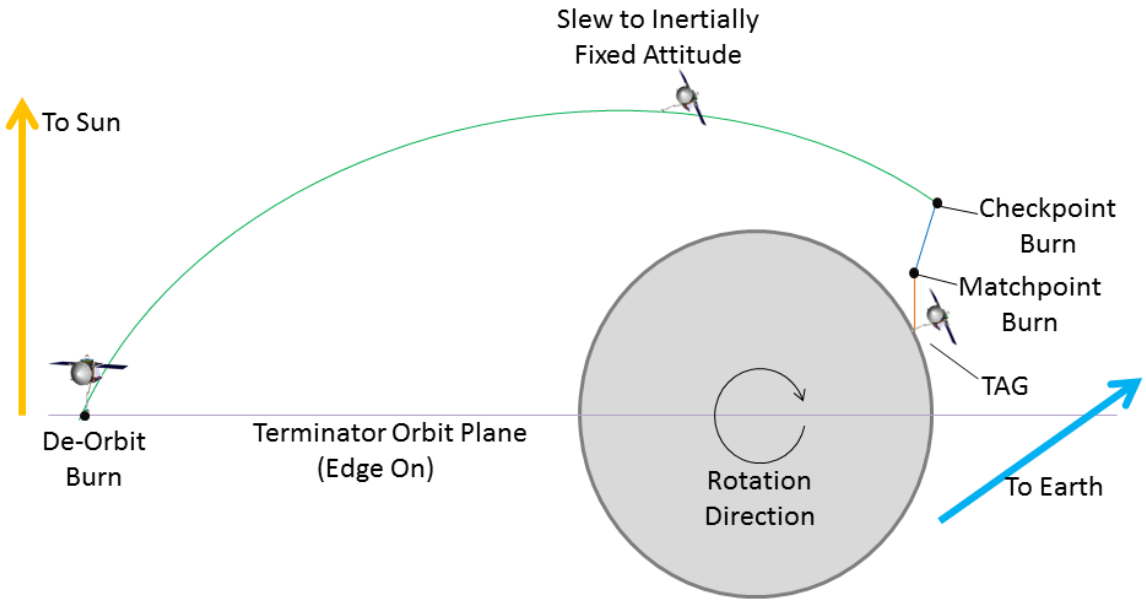

Figure 1. TAG Trajectory Sequence Following the De-Orbit Maneuver

The de-orbit maneuver will be a turn-burn-turn maneuver, meaning that the spacecraft will slew to point the main thrusters in the burn direction, fire the thrusters, then slew back. Before and after the de-orbit burn, the spacecraft attitude is set to point the solar arrays at the sun.

One hour before arriving at the Checkpoint position, the spacecraft slews to the inertially-fixed TAG attitude; this attitude is maintained for the remainder of the TAG sequence. The TAG attitude is determined by calculating the surface normal vector at the TAG site in the inertial frame at the nominal TAG time and aligning the TAGSAM arm with that normal vector.

When the Checkpoint position is reached, the Checkpoint maneuver will be performed to cancel out the majority of the surface-relative lateral velocity and begin descending towards the surface.

The Checkpoint maneuver is a set of 3 burns in the body frame occurring sequentially. This maneuver mode allows the spacecraft to maintain its inertially-fixed attitude.

After 10 minutes, the spacecraft will reach the Matchpoint at an altitude of 45 m. The Matchpoint maneuver reduces the rate of descent sufficiently to achieve a TAG vertical velocity of 10 cm/s. Note that the Checkpoint and Matchpoint maneuvers are targeted together to achieve the ideal TAG conditions. TAG occurs approximately 8 minutes after the Matchpoint maneuver.

The TAG sequence targeting methodology is detailed in Figure 2. Trajectory design and targeting in this analysis is performed with STK (Systems Tool Kit) by Analytical Graphics, Inc.

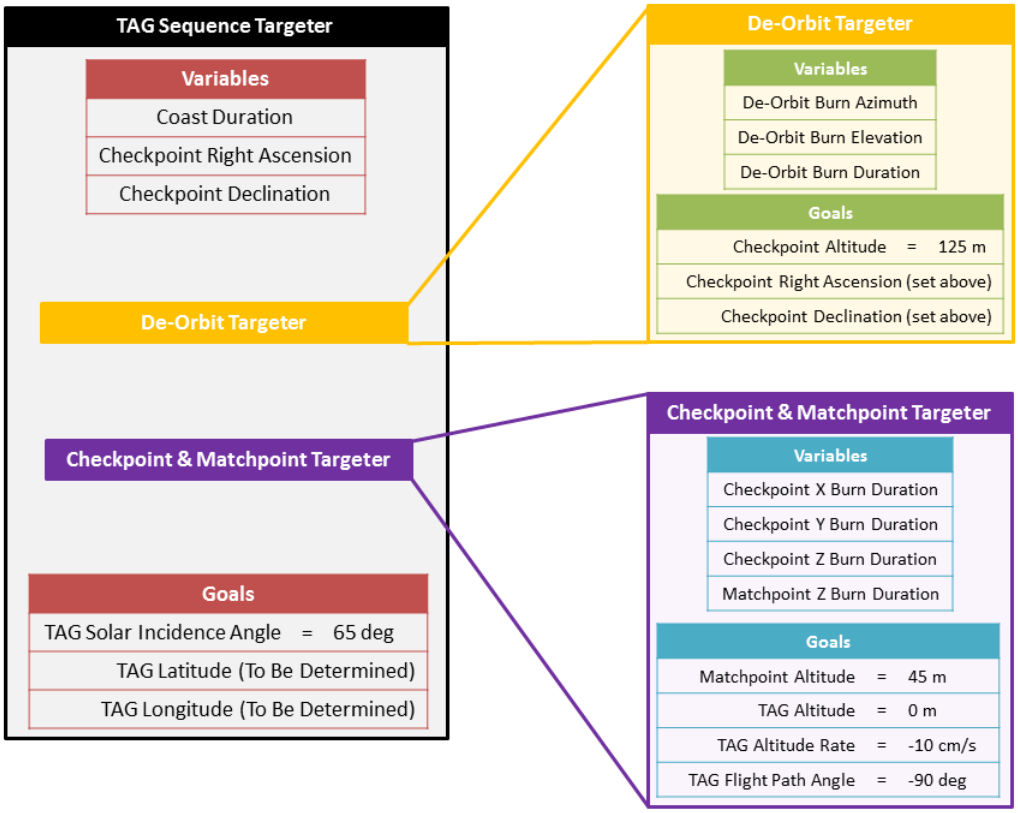

Figure 2. TAG Sequence Targeting Methodology

TAG REQUIREMENTS

TAG Position Error $\leq$ 25 m

The Flight Dynamics System has a requirement to deliver the spacecraft to within 25 m of a given TAG site with a Confidence Interval (CI) of 98.3%, which is approximately 2.85σ for a two-dimensional Gaussian distribution. The 98.3% CI is an allocation of the overall mission-level requirement on the probability of successfully acquiring a sample of at least 60 grams with a single TAG attempt. Three TAG attempts have been accounted for in the schedule and propellant budget in case the first attempt is deemed unsuccessful.

Trajectory Timing-Based Attitude Error $\leq 4^\circ$

The TAGSAM (Touch And Go Sample Acquisition Mechanism) head is hinged to allow up to 15° of tilt during TAG. If this angle is exceeded, the TAGSAM head will not be able to lay flat on the surface and the sample acquisition may be unsuccessful. In order to avoid exceeding this 15° limit, 14° have been allocated to local surface variations within 25 m of the TAG site, 3° have been allocated to spacecraft attitude control errors, and 4° have been allocated to trajectory timing-based attitude errors. The Root-Sum-Square (RSS) of the allocated angles is 14.87°, which leaves a small amount of unallocated margin. Since the TAG attitude is inertially-fixed and the asteroid is rotating, deviations in the time of TAG due to trajectory dispersions will result in an angular offset between the surface normal and the nominal spacecraft attitude, as illustrated in Figure 3.

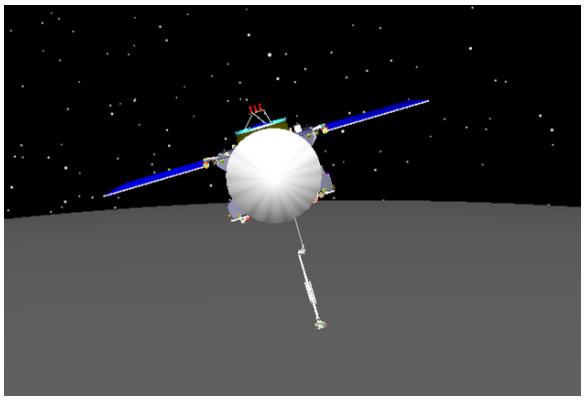

Figure 3. Example of Angular Offset Between Surface Normal and Spacecraft Attitude

Horizontal Velocity Error $\leq$ 2 cm/s

The spacecraft has a maximum tip-over angle of 45°, which if exceeded could cause the spacecraft to land on its side on the asteroid's surface. If the TAG site has a high surface friction, a high horizontal velocity during TAG can result in excessive tipping. The maximum horizontal velocity was chosen to be 2 cm/s to meet the maximum tip-over requirement with margin.

To prevent the spacecraft from tipping over during TAG, the attitude control system will be actively controlling the spacecraft attitude with reaction wheels. If the attitude rates exceed the capability of the wheels, thrusters will be engaged to provide the necessary control authority to protect the spacecraft.

Vertical Velocity Error $\leq$ 2 cm/s

Another potential cause of excessive tipping is if the spacecraft experiences high vertical velocity combined with a high TAG angle. The maximum vertical velocity has been set to 12 cm/s to meet the tip-over requirement. The vertical velocity must be greater than 8 cm/s to provide sufficient contact time between the TAGSAM head and the asteroid surface for sample collection. Combining the minimum and maximum allowable vertical velocity, TAG is targeted to occur with 10 cm/s of vertical velocity and is required to have no more than $\pm$ 2 cm/s of vertical velocity error.

MONTE CARLO ANALYSIS

A thorough Monte Carlo analysis is required to verify the ability of the TAG methodology to meet requirements. MATLAB (by MathWorks, Inc.) is used to drive the Monte Carlo analysis by automating the inputs to the STK scenario and applying the various perturbations to the nominal trajectory.

For this analysis, a spherical asteroid is assumed to maintain generality. TAG latitudes are chosen at the equator, -45°, and 75° to cover a range of scenarios. The asteroid spin axis is set to 180° away from the ecliptic normal, which is the best estimate provided by radio astronomers. The nominal asteroid gravitational parameter (GM) value is 4.16 m^3/s^2, but current uncertainty in the estimates of asteroid density and size yield bounding GM values of 2.93 m^3/s^2 (low) and 6.6249 m^3/s^2 (high).

NAVIGATION UNCERTAINTY AND MANEUVER EXECUTION ERRORS

Initial orbit uncertainty is provided by the navigation team. Simulated radiometric range and Doppler measurements are combined with simulated optical navigation based on asteroid surface landmark tracking to generate covariance information for each of the aforementioned three GM values. Included error sources are measurement noise, ground station location knowledge errors, optical navigation pointing uncertainty, maneuver execution errors from previous burns, asteroid ephemeris errors, and errors in force modeling for asteroid gravity and solar radiation pressure. The resulting 3σ navigation uncertainty is presented in Table 1.

Table 1. 3σ Navigation Uncertainty

	Position Uncertainty			Velocity Uncertainty		
	Radial (m)	In-Track (m)	Cross-Track (m)	Radial (mm/s)	In-Track (mm/s)	Cross-Track (mm/s)
Low GM	1.040	2.750	0.718	0.133	0.060	0.049
Nominal GM	0.529	3.132	0.633	0.173	0.035	0.077
High GM	0.686	4.039	1.195	0.326	0.058	0.040

During the TAG sequence each maneuver will be performed with the ACS thrusters and will impart a change in velocity ($\Delta\vec{v}$) between 1 cm/s and 20 cm/s in magnitude. The small magnitudes of these maneuvers drive the proportional errors to be larger than typical maneuver execution errors. The following values are 3σ accuracies:

Orbit Departure Maneuver Accuracy (Turn-Burn-Turn Maneuvers):

- Magnitude Error: 0.3 mm/s combined via RSS with 1.5% of $\Delta\vec{v}$ magnitude.
- Transverse Error: 0.3 mm/s + 2.5% of total $\Delta\vec{v}$ magnitude.

Checkpoint and Matchpoint Maneuver Accuracies (Vector Maneuvers):

- $\pm X$ and $\pm Y$ spacecraft body directions:
  - Magnitude Error: 0.3 mm/s combined via RSS with 5% of $\Delta\vec{v}$ magnitude.
  - Transverse Error: 0.3 mm/s + 10% of total $\Delta\vec{v}$ magnitude.
- $\pm Z$ spacecraft body directions:

– Magnitude Error: 0.3 mm/s combined via RSS with 5% of $\Delta\vec{v}$ magnitude.
– Transverse Error: 0.3 mm/s + 2.5% of total $\Delta\vec{v}$ magnitude.

ORBIT DISPERSIONS

Results of Monte Carlo analysis for an array of combinations of latitude and GM values with the error sources described previously are shown in Table 2. With initial state errors and de-orbit maneuver execution errors, the dispersions at the Checkpoint grow to 52-79 meters (3σ) along the principal axis of the covariance matrix. Adding in the maneuver execution errors at Checkpoint causes the dispersions to grow by approximately 10% at Matchpoint. When the trajectories are propagated to the asteroid surface, the radial error component becomes irrelevant and we are left with 2 dimensions of dispersion across the surface. The last column of Table 2 shows that this strategy does not meet the requirement to deliver the spacecraft to within 25 m of a given TAG site with a CI of 98.3%.

Table 2. Monte Carlo Results for TAG Accuracy for Various Latitudes and Asteroid GM Values

	Checkpoint Dispersions 3σ (m)	Matchpoint Dispersions 3σ (m)	TAG Dispersions 98.3% CI (m)
0° Latitude, Low GM	58.07	63.66	63.00
0° Latitude, Nominal GM	65.02	71.66	70.04
0° Latitude, High GM	79.95	89.29	84.86
-45° Latitude, Low GM	52.06	57.22	55.42
-45° Latitude, Nominal GM	57.31	63.33	60.27
-45° Latitude, High GM	68.79	76.96	70.39
75° Latitude, Low GM	53.93	59.22	55.93
75° Latitude, Nominal GM	56.56	62.21	57.32
75° Latitude, High GM	63.61	70.30	60.82

These inadequate results suggest the need for a method to reduce or correct the errors at Checkpoint. Due to the limited timeline and the approximately 20 minute round-trip light time delay on communications, ground-based updates would not be very helpful. After several trade studies of various levels of on-board autonomy, we selected a simple, yet elegant, closed-loop control algorithm based on Light Detection And Ranging (LIDAR) measurements.

LIDAR MEASUREMENTS

The spacecraft will be carrying a LIDAR instrument on-board, which provides surface range measurements. When the spacecraft slews to the inertially-fixed TAG attitude during the TAG sequence, the LIDAR will be pointed off into space. Approximately 25 minutes before the Checkpoint is reached, the LIDAR beam will cross the limb of the asteroid and the LIDAR instrument will begin receiving measurements. During this 25 minute span between limb crossing and the Checkpoint, LIDAR measurements will be used to predict the Checkpoint state. This scenario is depicted in Figure 4.

The first measurement that will be used is the LIDAR Range Threshold Crossing time. When the LIDAR beam crosses the limb, the range will be approximately 250 m and will quickly decrease.

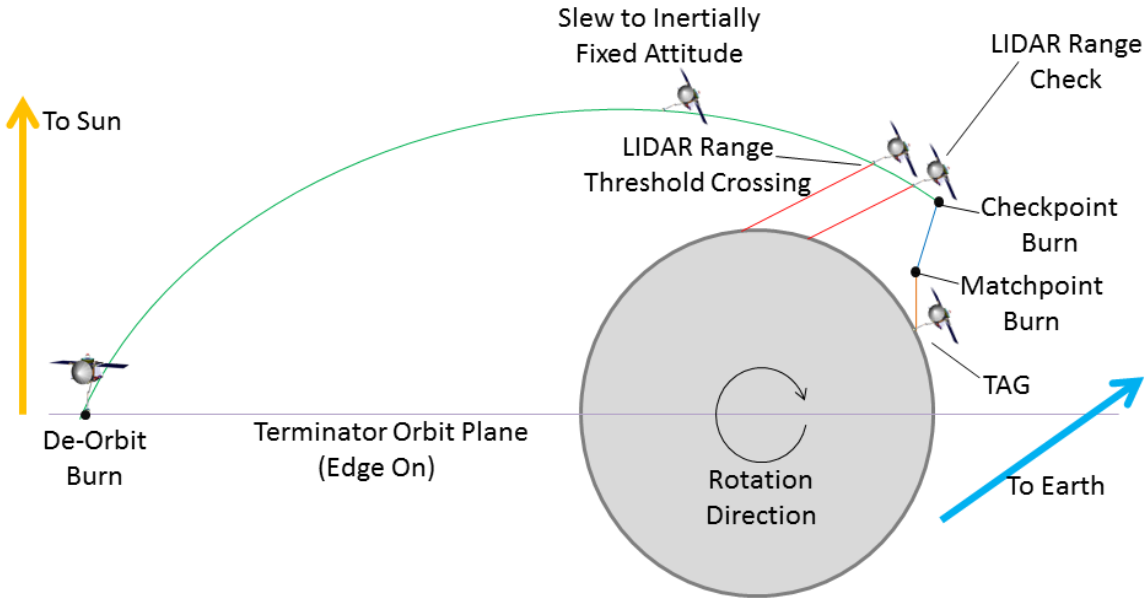

Figure 4. TAG Trajectory Sequence Following the De-Orbit Maneuver with LIDAR Measurements

For a specific trajectory, a threshold value will be chosen based on when the LIDAR beam will be 70° away from the surface normal vector. This LIDAR Range Threshold value is generally around 200 meters, and the crossing occurs a few minutes after limb crossing. Measuring the time at which this range crossing occurs provides a measurement of in-track orbit dispersions.

The second measurement will be the LIDAR Range Check distance. Two minutes before the nominal Checkpoint time, a LIDAR range measurement will be taken. Since the Checkpoint is nominally 125 m above the surface, the LIDAR Range Check distance will generally be close to 130 m. Deviations in this range value provide a measurement of radial orbit dispersions.

The 3σ maximum instrument noise expected for the LIDAR measurement is 10 cm + 1% of the actual range value. However, the measurements received on-board will also have "errors" (with respect to the actual distance to the mean asteroid surface) due to topographical altitude variations in the particular area of the asteroid surface against which the LIDAR is measuring.

SURFACE VARIATION

Modeling the asteroid as a self-affine structure, the standard deviation of the variation of the surface σ over a baseline distance L is given by

$$\sigma = \sigma_0 \left(\frac{L}{L_0} \right)^H \tag{1}$$

where L_0 is always 1 m, σ_0 is a normalizing constant, and H is the Hurst exponent. The values for σ_0 and H are fit to measured data. The baseline distance L is the distance between two points on the surface, which for our purposes are an expected surface location and an actual observed surface location. The baseline distance is the standard deviation of the orbit uncertainty combined with the pointing uncertainty projected onto the surface of the asteroid, which is encompassed by $L = 20$ m.

As a worst-case analog to our asteroid, the rough highlands of the asteroid 25143 Itokawa (1998 SF_{36}) were examined. Based on the data presented in Ref. 2, surface variation values in the rough highlands can be fit to generate the values $H = 0.36$, and $\sigma_0 = 0.89$ m. Combining those numbers with the aforementioned baseline distance yields a surface variation of $\sigma = 2.6$ meters (7.8 m 3σ). For comparison, the Hayabusa mission touched down in the smooth lowlands on Itokawa in an area known as the MUSES-C regio, which has a variation of 1 m over our baseline distance.

Existing radar polarization data provides reason to believe that RQ_{36} is smoother than Itokawa, as presented in Ref. 3. Using data from ground-based observations, the following surface variation values were derived for the expected RQ_{36} surface: $H = 0.72$ and $\sigma_0 = 0.13$ m. Combining those numbers with the baseline distance yields a surface variation of $\sigma = 1.1$ m (3.3 m 3σ).

GUIDANCE

The two LIDAR measurements described previously provide radial and in-track orbit information. To maintain simplicity in the on-board software, the relationship between these LIDAR measurements and the Checkpoint state is fit to a two-dimensional 2^{nd} order polynomial in which t is the LIDAR Range Threshold Crossing time error and r is the LIDAR Range Check error. The polynomial equation is

$$X_i = a_1 t^2 r^2 + a_2 t r^2 + a_3 r^2 + a_4 t^2 r + a_5 t r + a_6 r + a_7 t^2 + a_8 t + a_9 \tag{2}$$

where the subscript i refers to the six elements of the spacecraft's Cartesian state vector, i.e., $X_1 = x$, $X_2 = y$, $X_3 = z$, $X_4 = \dot{x}$, and so on.

Since we are predicting the entire 6-element inertial Cartesian state of the spacecraft center of mass at Checkpoint, we require 6 independent polynomials. These polynomials may be written in matrix notation as

$$\begin{bmatrix} x \\ y \\ z \\ \dot{x} \\ \dot{y} \\ \dot{z} \end{bmatrix} = \begin{bmatrix} a_{1,1} & a_{1,2} & a_{1,3} & a_{1,4} & a_{1,5} & a_{1,6} & a_{1,7} & a_{1,8} & a_{1,9} \\ a_{2,1} & a_{2,2} & a_{2,3} & a_{2,4} & a_{2,5} & a_{2,6} & a_{2,7} & a_{2,8} & a_{2,9} \\ a_{3,1} & a_{3,2} & a_{3,3} & a_{3,4} & a_{3,5} & a_{3,6} & a_{3,7} & a_{3,8} & a_{3,9} \\ a_{4,1} & a_{4,2} & a_{4,3} & a_{4,4} & a_{4,5} & a_{4,6} & a_{4,7} & a_{4,8} & a_{4,9} \\ a_{5,1} & a_{5,2} & a_{5,3} & a_{5,4} & a_{5,5} & a_{5,6} & a_{5,7} & a_{5,8} & a_{5,9} \\ a_{6,1} & a_{6,2} & a_{6,3} & a_{6,4} & a_{6,5} & a_{6,6} & a_{6,7} & a_{6,8} & a_{6,9} \end{bmatrix} \begin{bmatrix} t^2 r^2 \\ t r^2 \\ r^2 \\ t^2 r \\ t r \\ r \\ t^2 \\ t \\ 1 \end{bmatrix} \tag{3}$$

For each trajectory, Monte Carlo runs without LIDAR errors are used to calibrate the 54 coefficients of the matrix in Eq. 3. This calibration is achieved with a least-squares fit of all perturbed Checkpoint states with their respective t and r values. Table 3 presents the results of calibration. The first three columns are the radial, in-track, and cross-track position dispersions at Checkpoint, and the last three columns are the errors in the prediction of the Checkpoint position using the polynomial fit. Since these results do not include any errors in the LIDAR measurements, the Monte Carlo run results will have larger errors in the predicted Checkpoint states.

Differencing the predicted with the nominal Checkpoint state provides a position error and a velocity error, which can be used to adjust the Checkpoint and Matchpoint maneuvers. Since these

events happen over a short time period in a microgravity environment, we treat the governing dynamics as being linear. The following is the procedure for on-board adjustment of the maneuvers.

1. Velocity deviations are subtracted from the nominal Checkpoint maneuver.
2. Position deviations are divided by the time to Matchpoint and then subtracted from the Checkpoint maneuver.
3. The position deviation correction above is also added to the Matchpoint maneuver to cancel out the extra velocity.
4. The Checkpoint maneuver start time is adjusted to re-center it about the nominal burn center time.
5. The Matchpoint burn end time is adjusted to end at the nominal burn end time.

Table 3. Polynomial Fit Calibration Results for Checkpoint Prediction Errors

	Checkpoint Position Errors 3σ (m) Radial	Checkpoint Position Errors 3σ (m) In-Track	Checkpoint Position Errors 3σ (m) Cross-Track	Checkpoint Prediction Errors 3σ (m) Radial	Checkpoint Prediction Errors 3σ (m) In-Track	Checkpoint Prediction Errors 3σ (m) Cross-Track
0° Latitude, Low GM	23.63	53.56	9.01	0.24	0.41	8.65
0° Latitude, Nominal GM	26.66	59.77	8.28	0.21	0.29	7.94
0° Latitude, High GM	34.13	73.51	7.75	0.33	0.38	7.44
-45° Latitude, Low GM	19.92	49.43	7.74	0.11	0.25	7.42
-45° Latitude, Nominal GM	21.76	54.43	6.73	0.10	0.26	6.45
-45° Latitude, High GM	26.76	64.88	5.86	0.11	0.30	5.68
75° Latitude, Low GM	17.11	49.28	4.47	0.13	0.41	4.18
75° Latitude, Nominal GM	17.49	51.48	3.72	0.06	0.37	3.50
75° Latitude, High GM	19.28	57.40	3.01	0.05	0.34	2.92

The plots in Figure 5 show the results of the guidance algorithm on a single Monte Carlo run of one thousand trajectories with the highest set of blue dots being the Checkpoint positions, the middle set of blue dots being the Matchpoint positions, and the lowest set being the TAG positions. Figure 5(a) shows the trajectories without the implementation of on-board guidance, and Figure 5(b) shows the improvement gained with on-board guidance. Actual numbers will be presented in the Results section.

SUMMARY OF ERROR SOURCES

The diagram in Figure 6 incorporates all of the error sources detailed previously and shows the difference between a nominal trajectory (the dashed line) and a single perturbed trajectory (the solid line). The initial state is perturbed based on the navigation uncertainty, then the de-orbit burn is applied with maneuver execution errors added. The spacecraft slews to an inertially-fixed attitude that is based on the surface normal vector from the nominal TAG location. An asteroid radius error is applied based on the surface variation model being used, and the LIDAR Range Threshold Crossing time is obtained. Two minutes before the nominal Checkpoint time, the LIDAR Range Check value is obtained and a random range error is added to it based on the surface variation model being used. The guidance algorithm calculates the predicted Checkpoint state and updates the Checkpoint and Matchpoint burns accordingly. Maneuver execution errors are added to each burn, and the spacecraft is propagated to the asteroid surface. All of the errors that are applied to the trajectory are zero-mean Gaussian errors.

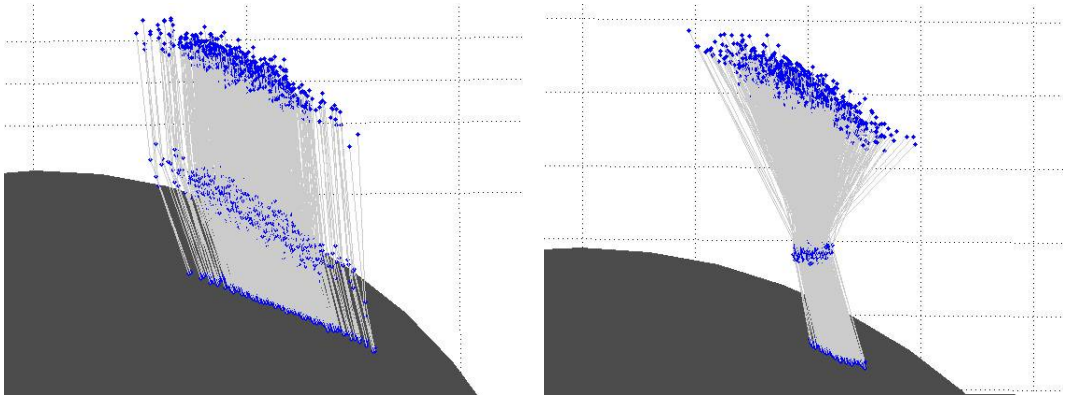

(a) TAG Trajectories Without On-Board Guidance (b) TAG Trajectories With On-Board Guidance

Figure 5. Monte Carlo Results (1000 Cases) for TAG Sequence Trajectories Without and With On-Board Guidance

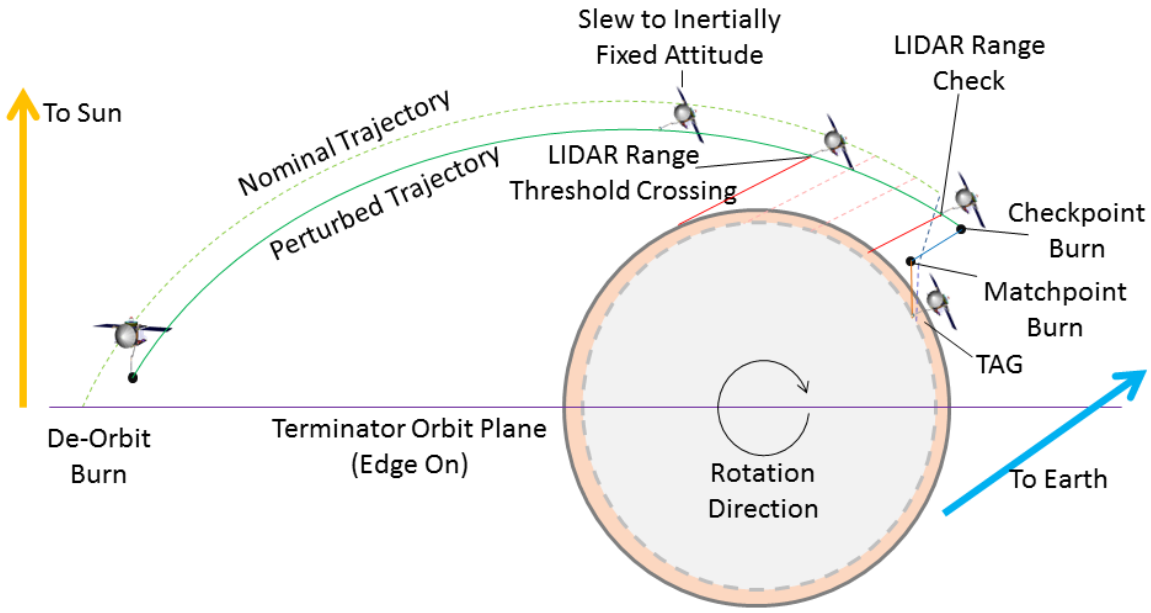

Figure 6. TAG Trajectory Sequence With Error Sources Illustrated

RESULTS

Table 4 presents the results of the Checkpoint prediction algorithm with all of the error sources included. The first three columns are the 3σ prediction errors in the radial, in-track, and cross-track directions using the expected RQ36 surface variation model. The last three columns show the prediction errors using the worst-case Itokawa-based surface variation model.

Continuing down to the surface of the asteroid, Table 5 presents all of the TAG results. The first

Table 4. Checkpoint Prediction Algorithm Results With All Error Sources Included

	Expected RQ_{36} Surface Model Errors 3σ (m) Radial	Expected RQ_{36} Surface Model Errors 3σ (m) In-Track	Expected RQ_{36} Surface Model Errors 3σ (m) Cross-Track	Itokawa-Based Surface Model Errors 3σ (m) Radial	Itokawa-Based Surface Model Errors 3σ (m) In-Track	Itokawa-Based Surface Model Errors 3σ (m) Cross-Track
0° Latitude, Low GM	4.71	9.25	8.70	10.28	19.29	8.89
0° Latitude, Nominal GM	4.70	8.70	7.99	10.25	18.13	8.15
0° Latitude, High GM	4.94	8.45	7.48	10.72	17.59	7.59
-45° Latitude, Low GM	4.17	7.99	7.51	9.18	16.63	7.71
-45° Latitude, Nominal GM	4.16	7.51	6.52	9.17	15.61	6.66
-45° Latitude, High GM	4.23	7.11	5.72	9.30	14.78	5.79
75° Latitude, Low GM	3.96	8.15	4.22	8.79	16.92	4.34
75° Latitude, Nominal GM	3.93	7.31	3.53	8.71	15.14	3.63
75° Latitude, High GM	3.94	6.61	2.94	8.72	13.68	2.97

column is the 98.3% CI TAG ellipse* obtained from Monte Carlo runs using the expected RQ_{36} surface variation model, followed by the results from the Itokawa-based surface variation model. The middle two columns show the 3σ TAG velocity errors relative to the spacecraft body frame, which are equivalent to the RSS of the horizontal and vertical velocity errors described previously. The last two columns show the timing-based attitude errors as described previously.

Table 5. TAG Results for Expected RQ_{36} and Itokawa-Based Surface Models

	98.3% CI TAG Ellipse Expected RQ_{36} Surface (m)	98.3% CI TAG Ellipse Itokawa-Based Surface (m)	3σ Body-Relative Velocity Expected RQ_{36} Surface (cm/s)	3σ Body-Relative Velocity Itokawa-Based Surface (cm/s)	3σ Nominal Attitude Error Expected RQ_{36} Surface	3σ Nominal Attitude Error Itokawa-Based Surface
0° Latitude, Low GM	8.627	16.597	1.158	1.291	2.713°	3.992°
0° Latitude, Nominal GM	8.107	15.113	1.063	1.110	2.740°	3.930°
0° Latitude, High GM	8.339	13.946	1.127	1.153	3.173°	4.320°
-45° Latitude, Low GM	8.656	15.752	1.056	1.198	1.947°	2.541°
-45° Latitude, Nominal GM	8.522	14.605	1.067	1.198	2.043°	2.617°
-45° Latitude, High GM	9.320	13.808	1.216	1.329	2.419°	2.971°
75° Latitude, Low GM	10.507	17.874	1.201	1.351	0.854°	1.023°
75° Latitude, Nominal GM	10.610	16.437	1.241	1.370	0.937°	1.108°
75° Latitude, High GM	12.362	15.999	1.382	1.504	1.200°	1.379°

The results clearly show that all TAG requirements are met for the expected RQ_{36} surface variation model. Using the worst-case Itokawa model, all requirements are met with the exception of a single case (0° latitude, high GM) that slightly exceeds the 4° attitude error allocation. We could formally change our allocation to cover this case, but we found that to be unnecessary due to the overly conservative nature of the worst-case Itokawa surface variation model. However, if we need to handle this case we certainly could because we still have unallocated margin, and we could increase our allocation to 4.47° and still fit within the overall requirement of 15° for the TAGSAM head.

CONCLUSIONS

Designing and implementing a TAG trajectory sequence to bring the spacecraft down to the surface of near-Earth asteroid (101955) 1999 RQ_{36} accurately and safely for successful regolith sample

*"TAG ellipse" refers to the longest dimension (i.e., semi-major axis) of a bounding ellipse fit to the dispersion of simulated points of spacecraft contact on the asteroid's surface. The center of this ellipse is generally near the desired point of contact. We therefore desire that the size of the 98.3% CI TAG ellipse be ≤ 25 m to satisfy requirements.

collection will be one of the most challenging tasks of the OSIRIS-REx mission. After analysis including expected orbit covariance and all other anticipated error sources demonstrated that TAG requirements could not be met by simply applying pre-computed maneuvers based on nominal state information, the OSIRIS-REx Flight Dynamics team endeavored to develop additional procedures and algorithms to augment the TAG maneuver sequence without requiring on-board autonomy beyond what is achievable by the spacecraft.

The outcome of those efforts has been detailed in this paper and the key result is a simple, yet elegant, closed-loop on-board guidance scheme that utilizes a two-dimensional polynomial relationship between the Cartesian spacecraft state (position and velocity) predictions and LIDAR measurements. The array of coefficients for this polynomial representation can be calibrated in a straightforward fashion and uploaded to the spacecraft, and the simple linear maneuver correction calculations based on the polynomial model are easily performed and applied on-board in real-time.

This innovative on-board algorithm has been demonstrated in thorough Monte Carlo simulations to dramatically reduce the dispersions on achieved asteroid surface contact location (relative to the desired surface contact location), surface-relative velocity error, and spacecraft attitude error at surface contact, bringing all of those quantities well within the mission requirements for a successful TAG. The OSIRIS-REx Flight Dynamics team will continue testing and refining the guidance algorithms and TAG sequence design with increasingly higher fidelity models to ensure successful sample collection at RQ_{36}.

ACKNOWLEDGMENT

This work is supported by the OSIRIS-REx Asteroid Sample Return Mission project, for which Dr. Dante Lauretta is the Principal Investigator, within NASA's New Frontiers program. The authors are grateful for contributions to this work by the OSIRIS-REx Flight Dynamics team and other OSIRIS-REx subsystem teams. The authors are also appreciative of support and technical input from the OSIRIS-REx Science team liaisons to the Flight Dynamics team, Dr. Steven Chesley and Dr. Daniel Scheeres.

REFERENCES

[1] D. S. Lauretta and OSIRIS-Rex Team, "An Overview of the OSIRIS-REx Asteroid Sample Return Mission," *Lunar and Planetary Institute Science Conference Abstracts*, Vol. 43 of *Lunar and Planetary Inst. Technical Report*, Mar. 2012, p. 2491.

[2] O. S. Barnouin-Jha, A. F. Cheng, T. Mukai, S. Abe, N. Hirata, R. Nakamura, R. W. Gaskell, J. Saito, and B. E. Clark, "Small-scale topography of 25143 Itokawa from the Hayabusa laser altimeter," *Icarus*, Vol. 198, No. 1, 2008, pp. 108 – 124.

[3] L. A. Benner, S. J. Ostro, C. Magri, M. C. Nolan, E. S. Howell, J. D. Giorgini, R. F. Jurgens, J.-L. Margot, P. A. Taylor, M. W. Busch, and M. K. Shepard, "Near-Earth asteroid surface roughness depends on compositional class," *Icarus*, Vol. 198, No. 2, 2008, pp. 294 – 304.